



Contents lists available at ScienceDirect

Journal of Volcanology and Geothermal Research

journal homepage: www.elsevier.com/locate/jvolgeores

Underwater and drone based photogrammetry reveals structural control at Geysir geothermal field in Iceland

Thomas R. Walter ^{a,*}, Philippe Jousset ^a, Masoud Allahbakhshi ^a, Tanja Witt ^a, Magnus T. Gudmundsson ^b, Gylfi Páll Hersir ^c

^a GFZ German Research Centre for Geosciences, Telegrafenberg, 14473 Potsdam, Germany

^b Nordvulk, Institute of Earth Sciences, University of Iceland, Askja, Sturlugata 7, IS-101 Reykjavík, Iceland

^c Iceland GeoSurvey (ÍSOR), Grensásvegur 9, 108 Reykjavík, Iceland

ARTICLE INFO

Article history:

Received 11 July 2017

Received in revised form 11 December 2017

Accepted 15 January 2018

Available online xxxx

Keywords:

Geysir geothermal field

Hydrothermal eruption

Strokkur

Geysir

Drone monitoring

Volcano earthquake interaction

ABSTRACT

Geysers are local hydrothermal vents with periodic gas bubble driven explosions at the surface. Little is known, however, on the control on distribution, the dynamics and the geometry of the conduits of geysers. To better understand the link between the deep and surface expression at the Geysir geothermal field, Iceland, a detailed analysis of the spatial distribution of the thermal expressions, and their relationship to the tectonic framework was carried out. By use of high resolution unmanned aerial vehicle (UAV) based optical and radiometric infrared cameras, we are able to identify 364 distinct thermal spots distributed over the area. Close analysis of their arrangement yields a clustered appearance, following a preferred direction that is found to be consistent with the assumed tectonic trend in the area. Furthermore by using underwater cameras we are able to obtain for the first time detailed images from the two largest geysers at depths exceeding 20 m. Near to the surface, the conduit of the geysers are near circular, but at a depth of 9–12 m the shape changes into a crack-like elongated fissure. The elongation direction of these deep cracks is consistent with the identified thermal expression at the surface, highlighting a structural or even tectonic control at the Geysir geothermal field, which may also explain the susceptibility for seismically triggered activity changes.

© 2018 Elsevier B.V. All rights reserved.

1. Introduction

Geysers and thermal springs commonly developed in volcanic areas, are considered as volcano analogues (Balcerak, 2013; Kieffer, 1984) and are vivid manifestations of the earth cooling processes and geothermal fluid mobility through the shallow crust (Hurwitz and Manga, 2017; Rinehart, 1980), however the subsurface structure and conduit geometry remains often poorly constrained (Wu et al., 2017). While hot springs discharge the thermal water continuously, a geyser is characterized by intermittent eruption pulses, where in some places hot steam and water are violently expelled to tens of meters height above the ground surface. The regimes of geysers and hot springs have in common that they are subject to various changes in time and space, and might be controlled by volcanic activity, the tectonic and structural framework, stress changes and the conditions of fluid transfer through a permeable rock mass (Ingebretsen and Rojstaczer, 1993; Manga and Brodsky, 2006; Munoz-Saez et al., 2015b; Rojstaczer et al., 2008). Detailed mapping of the distribution of the surface expressions may allow obtaining an indirect glimpse into the structural relations beneath. Even though the

geysers and hot springs are often thought to be fault-controlled (Neale et al., 2016), physical modeling suggest that geysers may be rooted in narrow confined tubes, or in more complexly shaped conduits and interconnected reservoirs at depth (Dowden et al., 1991; Mackenzie, 1842). Direct observations of the deeper conduits and reservoirs is limited, however, due to high temperatures and the eruptive nature of the geysers. Video observations down to a depth of 14 m inside an emptying geyser conduit shortly after eruptions reveal a very complex geometry at Old Faithful (Hutchinson et al., 1997). Also at Geysers of El Tatio (Chile) and in the Geyser Valley (Kamchatka, Russia) underwater video records allowed identifying reservoirs at some meter depths (Belousov et al., 2013; Munoz-Saez et al., 2015b). However, the structural relevance for conduit formation has not been studied yet in detail.

One of the driving mechanisms for geyser eruptions is the change of pressure that occurs as water turns into steam (Dowden et al., 1991). Resulting complexities in the convection and overturn behavior, tremors occurring before and after explosions, and multiple thrusts have been investigated, which may also provide an analogue for volcanoes (Julian, 1998). Due to the safe access to geysers, particularities in spatial appearance, structural relations and conduit geometries can be investigated directly, which are otherwise difficult to study at volcanoes (Julian, 1998).

* Corresponding author.

E-mail address: twalter@gfz-potsdam.de (T.R. Walter).

Geysers are also associated with significant mineralization and interactions (Dunckel et al., 2009), which may affect the geometry of their conduits. Distribution of geysers and hot springs may be controlled by structural conditions (Neale et al., 2016) or by rock permeability, and investigated at high resolution using handheld (Malin et al., 2011) or airborne thermal imagery (Neale et al., 2016). Repeated thermal measurements and photographs could identify significant changes occurring at geysers and hot springs, interpreted to be mainly fracture dominated, associated with local permeability changes (Neale et al., 2016). Details of these local permeability changes are often difficult to ascertain however, and may be related to the local stress field, presence of fractures, or presence of impermeable layers (Pantaleo and Walter, 2014). Geysers and hot springs may even interact between themselves (Muñoz-Saez et al., 2015b). The distribution of geysers and hot springs at the surface may be complex, and display structures hidden in the underground, as described herein for the type locality of geysers.

The Geysir geothermal field in Iceland has repeatedly displayed changes following tectonic earthquakes, where earthquakes may enhance or shut down eruptive activity of geysers (Einarsson, 1967; Storm, 1888). In June 2000, a Mw6.5 and Mw6.3 earthquake couple occurred in South Iceland (Antonioli et al., 2006; Vogfjord, 2003) and was followed by micro earthquakes (Hjaltadóttir, 2009) identifying hidden faults nearby the Geysir geothermal field (Fig. 1). Also, the geyser area

showed an increase in thermal and eruption activity, as reported by eyewitnesses (Pálmsón, 2002). Therefore, an open question is whether the geysers and hot pots align in a similar fashion as the seismically identified hidden faults, and if a study of the conduit geometry can reveal in some way these structural fabrics. In this paper, we describe a detailed mapping work at the Geysir geothermal field, Iceland, with the aim to explore the spatial distribution and structural architecture of the geysers and hot springs. Our study is based on photogrammetry, by using drone based optical and infrared imaging. Results are analyzed and compared to underwater images obtained at the two largest geysers, revealing a relevant structural control affecting the distribution and alignment of geysers and hot springs in the area. Underwater observations have been realized at other geysers already, but so far could not clearly identify a structural control (Belousov et al., 2013; Hutchinson et al., 1997; Muñoz-Saez et al., 2015a).

1.1. Geysir geothermal field

Situated in Haukadalur, southern Iceland, the Geysir geothermal field is one of the most famous tourist attractions in Iceland, and fed by the geothermal reservoir of an upper Pleistocene volcano (Jones et al., 2007; Torfason, 1999). High temperature geothermal areas in Iceland are commonly driven by cooling igneous intrusive bodies in the

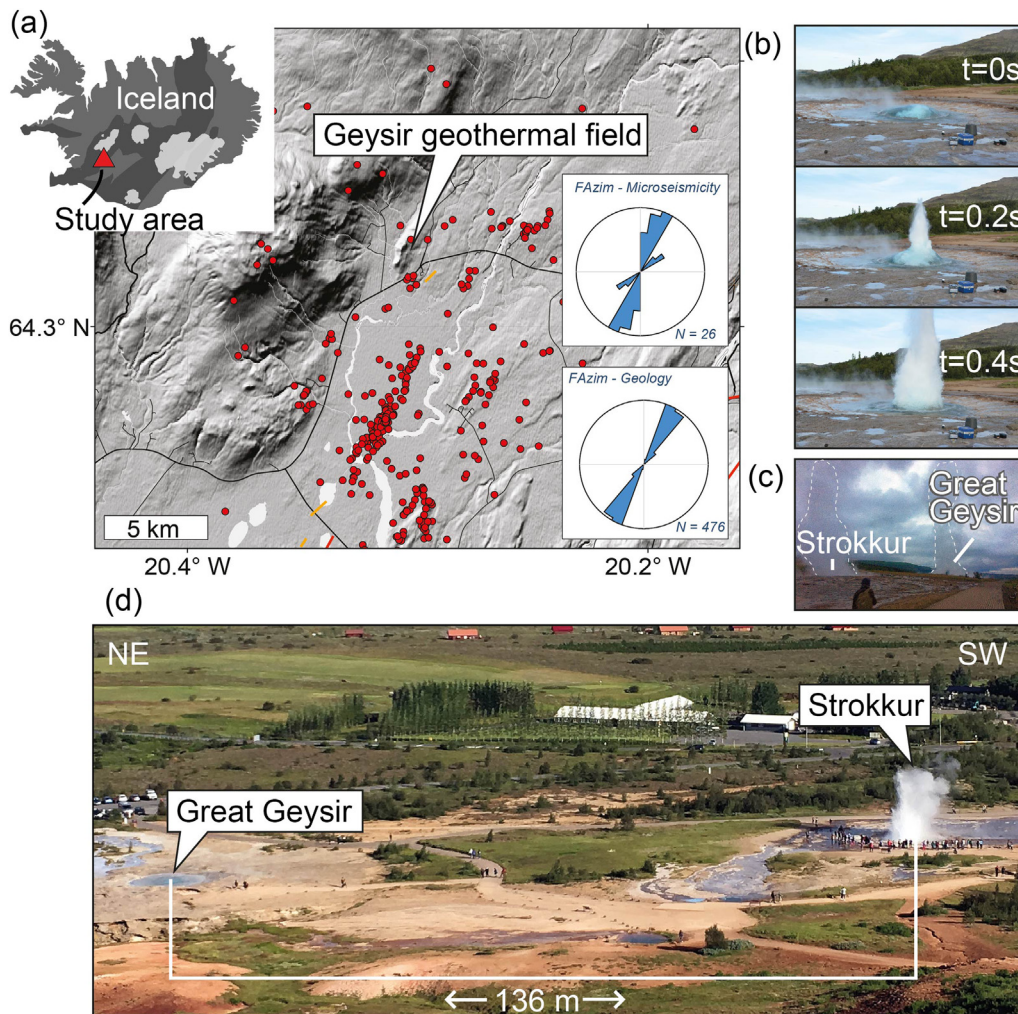


Fig. 1. a) Insert shows a map of Iceland and location of the Geysir geothermal field. Digital elevation map (Tandem-X data at 12 m resolution) and location of the geysers. Red dots are locations of microseismicity as triggered by a remote earthquake in the year 2000 (Hjaltadóttir, 2009). Rose diagrams show azimuths of seismically inferred faults (Hjaltadóttir, 2009), and azimuths from structural geologic mapping (Hjartardóttir et al., 2016). b) Time lapse (0.2 s interval) of a typical Strokkur eruption. c) Occurrence of weak double eruption at Strokkur and at Great Geysir observed in July 2016. Person for scale. d) Panoramic view over the Geysir field; distance between the two main geysers is 136 m. Map generated by authors using ArcMap 10.2 by ESRI (<http://www.esri.com/>). All photos taken during the field work by the authors.

shallow crust (Sigmundsson, 2006), this is also the case for the Geysir geothermal field. The Geysir field developed on the slope of a rhyolitic and repeatedly intruded topographic hill (Laugarfjall), a geology which is also found further west at Bjarnarfell (Torfason, 1999), implying that those parts have been connected before being tectonically separated. The ~3 km² large area hosts abundant hot springs that have been mapped and monitored thirty years ago (Torfason, 1985), and is punctuated by the Great Geysir and by Strokkur, both of which are pool geysers that are among the largest geysers on earth. Eruptions of Great Geysir have been infrequent in recent decades but they have reached 70–80 m height, whilst at Strokkur currently the maximum height of eruptions is about 30 m. Activity of these two geysers is variable, sometimes years or even decades without eruptions, and attempts to revive and control the activity have included addition of soap, drilling (in 1963 Strokkur was drilled), and changing the water table. Lowering of the water table by narrow outflow channels allowed increasing eruption rates, but nowadays eruptions at Great Geysir remain rare again, some years without eruptions reported (only few eruptions in 2016), whilst at Strokkur eruptions are much more frequent. During our 10-day field work in 2016, we observed 15–20 eruptions per hour at Strokkur (Fig. 1b) but only one weak eruption at Great Geysir (Fig. 1c). However, no continuous monitoring has been realized up to date, and reports are based on eye-witness accounts (Pálmasón, 2002), which is why details on the eruption changing intervals remain elusive.

Both geysers are fed through pipes, that are thought to be regular in shape and only slightly varying between 0.4 and 1 m in diameter and reaching down to 22 or 24 m depth (Pasvanoglu, 1998; Torfason, 1985; Torfason, 1999). The water temperatures at this depth are around 120 °C (Torfason, 1985), close to the boiling temperature (Bunsen, 1847), explaining why the water column can be unstable, leading to spontaneous eruption triggering. Above about 12 m depth, water temperatures decrease, with near constant temperatures of 85–95° C above the depth of 8 m (Torfason, 1985). Therefore, the geysers have two main temperature domains, ~85–95 °C in the upper zone, and ~120 °C at depth below 12 m. The bimodal temperature field has not been explained so far.

Although the geysers have been mentioned as early as in the 16th and 17th century literature (Nielsen, 1940), and repeatedly studied scientifically through centuries (Bart, 1940), detailed analysis on the dynamics and structure have been lacking (Pasvanoglu, 1998).

2. Data and methods

2.1. Close range aerial photogrammetry survey

Close range photogrammetry techniques are increasingly exploited in geosciences, thanks to the consumer friendly technical handling and robust and fast image processing technologies. As drones can carry cameras, the use of drones allowed acquisition of high resolution close range imaging data, even in difficult terrain, and allows to retrieve photomosaic and digital elevation data at unprecedented level of detail (Amici et al., 2013; Mancini et al., 2013; Nakano et al., 2014). Different carriers have been developed for the cameras, but multicopters allow a most flexible use (Carrivick et al., 2013) with a very small launch platform, that we found ideal to utilize at the geysers of Iceland. We analyze the retrieved images by modern computer vision approaches (James and Varley, 2012), and compute digital terrain models and thermal anomaly maps at unprecedented level of detail worldwide. The field campaign and accordingly all results presented are based on data acquired between 27 July and 5 August 2016.

We used light weight cameras mounted on a modified quadcopter drone DJI matrice 100 (Fig. 2a). This drone allows extended flight times of >30 min (with two LiPo packs) and simultaneous carrying of optical and thermal cameras. The drone was controlled by GPS, a live view transmitted to the operator, and the flight path predefined. We repeated the overflights during different daytimes, in order to test and

guarantee ideal image contrasts for the optical camera (daylight flight time best at 5:00 local time) and the infrared camera (cold night flight time at 3:00 local time). The flight altitude was between 80 and 140 m above the surface. The path was set to fly in loops at constant height above sea level, producing sufficient image over- and sidelapse. The optical camera used was a DJI Zenmuse X5R, a 16 megapixel micro four thirds aerial camera that was set to a time lapse frame rate of 2 frames per second, each image geolocated by GPS. The infrared camera used was a FLIR Tau 2 thermal camera at a fully radiometric resolution of 640 × 512 pixels (mean pixel size 17 cm), with a spectral band of 7.5–13.5 μm, also here each image geolocated by GPS. Temperatures derived from infrared imaging depend mainly on the emissivity of the object, the distance, and travel path to the camera sensor, solar reflection, viewing angle, and the presence of particles/gases in the electromagnetic radiation path (Spampinato et al., 2011). We measured the apparent temperature by assuming an emissivity of 0.95, a transmissivity of 0.7, an environmental and path temperature of 2 °C, and a humidity of 50%, based on a local weather station. A critical issue for infrared measurements are temporal variations in environmental conditions, which is why near simultaneous acquisitions are essential for any mapping projects. Therefore we use a high speed raw data frame grabber, Thermal Capture by TEAX Technologies, storing 60 images per second. The flight speed and altitude was defined in order to realize a minimum 80% overlap and sidelap between the images. Shaking due to the vibration of the drone was eliminated by a stabilizing gimbal. In total we could acquire 1500 optical and over 7000 infrared images covering 1.01 km² over the Geysir geothermal field.

2.2. Structure from motion

The optical and infrared images were grouped into two chunks and then photogrammetrically processed using the Structure from Motion (SfM) approach (Carrivick et al., 2013). The method allows us to reproduce high resolution three dimensional surfaces from two-dimensional images, and was realized using the commercial Photoscan Pro Software package (vs. 1.2.6). The requirements for the data are limited to a constant focal length, proper acquisition geometries, sufficient overlap in the images, which was over 80% in our study, and the measurement of GCPs (Ground Control points) for georeferencing purposes. Although our drone cameras were geotagged, we measured additionally 20 GCPs by using RTK-GPS (GPS/GNSS Leica 900 with a fixed reference station and rover type ATX900GG), and could identify all those points in the images, allowing further improvement of the geolocation of the data point clouds. The images are aligned by using corresponding pixel pairs in different images, also allowing to estimate the camera projections. Through matching we reconstruct the scene using tie points, generating a sparse point cloud of corresponding ground feature points in the original images. This information is further used for the dense reconstruction, leaving us in total with 88.4 Mio points for the optical images and 17.2 Mio points for the infrared data. The three dimensional models contain 5.9 Mio and 1.2 Mio faces for the optical and infrared data, leading to a digital elevation model with a pixel resolution of 6.57 and 23.8 cm, respectively. The orthomosaic was similarly calculated at 6.6 and 23.8 cm/pixel resolution.

We identified hot pots and perform spatial statistics by a cluster analysis using the ArcMap point density calculation function, with a search radius of 0.0001 degrees equivalent to 10 m in NS and 6 m in EW direction.

2.3. Underwater photogrammetry survey

Besides airborne photogrammetry, we obtained underwater video recordings. Video observations in geysers are challenging due to high temperatures and eruptions, but have been realized before elsewhere up to several meters depth and show the great value of studying a conduit directly (Belousov et al., 2013; Hutchinson et al., 1997; Munoz-Saez

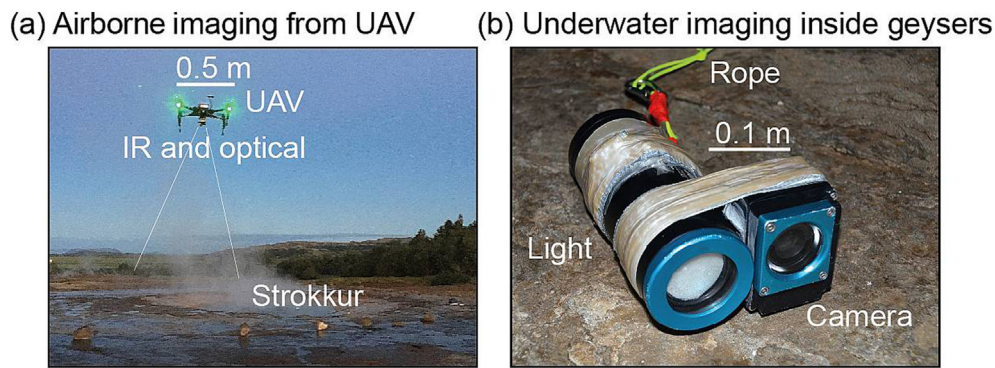


Fig. 2. Photogrammetric data acquisition. a) Quadcopter carrying infrared and optical camera overflights Strokkur geyser between eruptions, taking images at regular intervals along the pre-defined flight path. b) Underwater camera construction with bullet-proof (geyser-eruption-proof) deep water housing, left with LED light source, right with GoPro Hero 4 camera. Photos taken during the field work by the authors.

et al., 2015a). We compare the close range air photo analysis to views acquired from within the conduits of the two largest geysers, Strokkur and Great Geysir. To this aim we let a GoPro Hero 4 camera, 1920 × 1080 pixel resolution at 60 fps in low light video mode into the geysers. To protect the cameras against the water temperature of 120 °C, as well as eruptions and bubble collapses at depth, we used a GoBenthic housing, which is a bullet proof deep water aluminium enclosing, resisting over 240 bar overpressure. A similar housing (GPH-1750 m) was also used for the illumination, for which we used an 8000 lm LED source. The housings were fixed together at a dyneema line, and manually submersed up to 22 m depth for both geysers (Fig. 2b). Together with the underwater video records, we also measured the water temperature using PT100 sensors attached to a cable and logging at the surface. We measured the temperature between two eruptions, which could possibly differ slightly from temperatures during eruptions.

3. Results

3.1. Topography and lineaments

The digital elevation model retrieved from the drone camera covers the entire Geysir field, where for the optical images an area of 250,000 m² and for the infrared images an area of 810,000 m² is covered (Fig. 3). The digital elevation model shows details of the Geysir field at the eastern flank of Laugarfjall. The hill has an NE-SW elongation, similar to the azimuth of regional tectonic faults and alignments of microseismicity (Fig. 1). The region's high point is at the summit of Laugarfjall ~187 m a.s.l., and the geyser and hot spring area ranges mostly from 112 to 132 m a.s.l.. Therefore, although the Laugarfjall is a pronounced topographic ridge, the Geysir field is relatively well constrained at the surface, extending 620 m in the direction NNE-

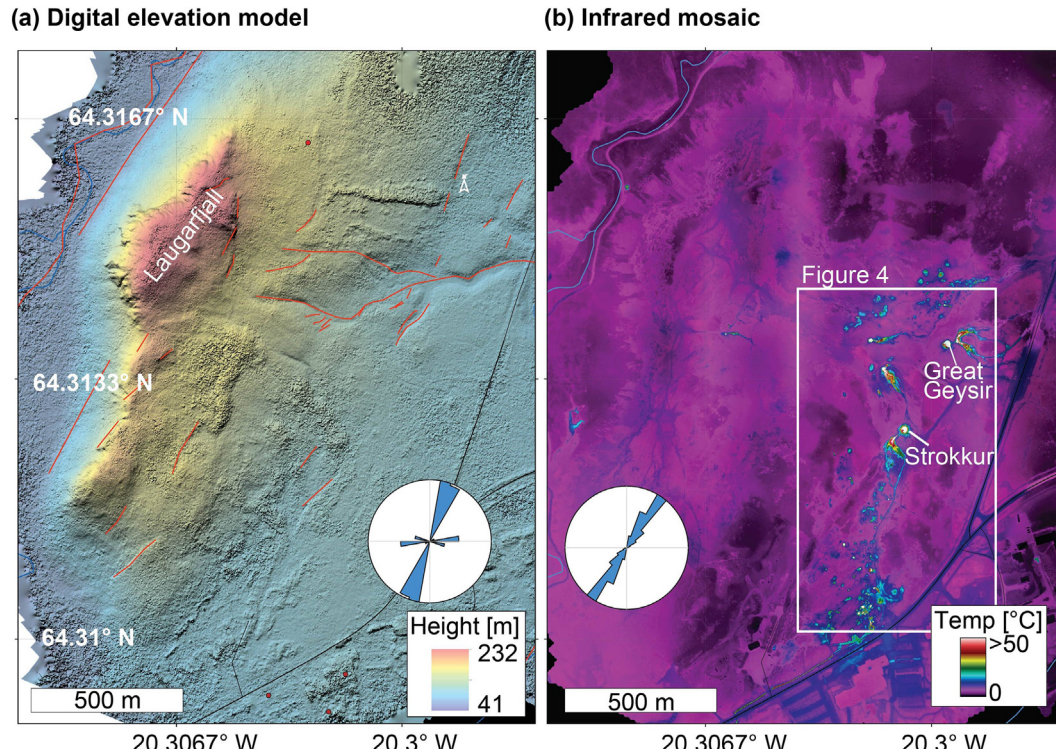


Fig. 3. Results from drone overflights. a) Structure from Motion calculation allows retrieving a 6-cm resolution digital elevation map. The Laugarfjall hill is clearly depicted, elongated NNE-SSW, steeply dipping on the west, and gently dipping at the geyser thermal field on the east. Lineaments identified from slope changes are shown by red lines, rose diagram reveals their azimuths oriented NNE-SSW (calculated at 5 m lineament increments). b) Thermal mosaic map of the same region as in (a), showing the expression of over 350 hot pots that are concentrated in the lower slopes of Laugarfjall, aligned in a direction NE-SW as the rose diagram reveals (calculated mean in 100 m search radius). The white box indicates the close-up views in Fig. 4. Map generated by authors using ArcMap 10.2 by ESRI (<http://www.esri.com/>).

SSW, but only 20 m vertically, which indicates that the bulk of activity is arranged slope-parallel.

The digital elevation map allows tracing a number of lineaments. Some of the lineaments are due to water streamlets and rivers, with a mean strike direction that is bimodally distributed, but dominates in the direction NNE-SSW as the rose diagram in Fig. 3a reveals. In addition, lineaments that show topographic expression might be due to tectonic processes or otherwise localized erosion; these strike NE-SW as indicated in Fig. 3b.

3.2. Spatial distribution of hot pots and geysers

The infrared mosaic derived from the thousands of individual images is shown in Fig. 3b. Overall, a large number of hot spots (individual thermal springs, geysers and hot pots) can be identified, where the size of the individual hot spots may vary significantly. Clearly identified are locations such as the large geysers Strokkur and Great Geysir, the hot springs Fata and Blesi (see white insert box in Fig. 3b and Fig. 4). The thermal field is largely obscured by the outflow channels at these productive locations. In the surrounding of the most productive geysers, we identify a virtual absence of smaller hot spots.

From the infrared mosaic we can identify over 364 well distinguished hot spots, with very variable distances between them ranging from decimeter to hundreds of meters at isolated locations. Such isolated locations are found at higher grounds of the southern ridge on Laugarfjall, but also west of Laugarfjall in the adjacent valley. Over 98% of all identified hot spots are located within the main area of 40,000 m². The hot spots often form clusters, as the density distribution map (Fig. 4) reveals. These clusters are arranged in NE-SW direction, and contain over 20 hotspots (clusters C1–C4, C6–C7), or about 10 hot spots (clusters C8–C14). Clusters are arranged in an eastern (C1–C7) and a western alignment (C8–C14), where the eastern one appears more active. Distance between the clusters is often only a few tens of meters, gaps of clusters exceeding 100 m are absent in the main hot spot area, with the exception near to the sites of Strokkur and Great Geysir (Fig. 4, center row). There, the absence of smaller hot spots is evident. One might speculate whether the punctuation at the Geysir field eventually closed other hot springs in the area. Therefore, hot fluids rising in the vicinity are channeled into these two feeder conduits.

To test a structural control at the depth of the larger geysers, we performed underwater video imaging. Overall, the image quality is very high for Great Geysir, and allows identifying the conduit geometry. At Strokkur, however, image qualities are lower, which is due to the constantly rising little gas bubbles, which by use of our LED light source appear as bright spots and blur the image. A summary, showing similarities and differences of the conduit geometries for both geysers is illustrated in Fig. 5. Underwater images taken at 5 m water depth (Fig. 5) show that the Great Geysir conduit is near circular at first, sinter-lined, and then becoming elliptically elongated ~12 m depth with an aspect ratio where the long axis is 4 to 5 times the short axis length; the long axis being north-south to northeast-southwest oriented, i.e. subparallel to the principal fault direction in the area. The sinter disappears at ~14 m depths.

The Strokkur pipe is first near circular, sinter-lined, then narrowing at depth and becomes elliptical at 9 m depth, lacking sinter, and widens again at 12 m depth. Closer views into the Strokkur pipe reveal that the vertex region of the major axis is crack-like (Fig. 5 at ~10 m), where the long axis is about 1.5 to 2 times the short axis length. Therefore, the Strokkur pipe is slightly less elliptical than the Great Geysir pipe, but still fracture controlled. Therefore, both geyser pipes are strongly elliptical at depth, the long axis being subparallel to the principal fault direction in the area. At even larger depths the images become more blurred because of convection and instability of the water column. However, the elliptical shape reappears at 16–18 m depth, and again clearly indicates a structural control, before at even larger depth the pipe direction changes and the geometry complicates. The pipe becomes slightly

inclined, dipping about 80 degrees, to the north. The geometry is no more elliptical. Although the turbulence at this depth is high, our underwater video observations reveal that the presence of bends in the conduit geometry and then the divergence into several paths. At the base big boulders are identified. Cavity-like embayments on the sides were further identified, possibly two or more channels (see Supplementary video), that could play a major role in the dynamics of geysers as proposed by independent studies (Belousov et al., 2013; Munoz-Saez et al., 2015b).

This profound change in the geometry, from circular near to the surface to crack-like at depth, is also reflected in the water temperature. Our temperature logs performed during the camera records, show that at 1 m water depth the Great Geysir temperature is 90 °C, and remains almost constant, rising only to 95 °C at 10 m depth. At this depth the temperature also starts rising, reaching 118 °C at 12 m depth, further increasing to 123.7 °C at 15 m depth and remains near constant until a depth of 22 m is reached. Similar at Strokkur, temperatures show a remarkable increase from 94 °C to 123 °C at >12 m depth, where the conduit narrows to a crack-like geometry (Fig. 5). Anomalies in the temperature field and the structure of the geyser pipe are therefore closely coupled.

4. Discussion

Structural analysis of geysers and distribution analysis of hot spots reveals the importance of fractures in the Geysir geothermal field of Iceland. We used photogrammetric techniques from drones and underwater, and identified structural relationships in the thermal and morphologic expression. The general distribution of the hot spots is aligned, but appears in clusters, whilst geysers are isolated and punctuated geothermal manifestations. Azimuthal trends of the hot spot clusters, of local lineaments, and of the topography are in agreement with the azimuthal trends of triggered seismicity in 2000 and regional tectonic lineaments, with important implications for understanding these remote triggering processes. Before discussing the geologic relevance of this work we summarize a number of limitations.

4.1. Limitations

We acquired drone based optical images during daylight and infrared images during night. This was necessary, as to provide sufficient illumination to the optical photos, and to reduce solar reflectance during the infrared survey. The daylight images, in fact, although of higher resolution than the infrared images, were subject to local artifacts especially near to Strokkur and along trails. This we interpret to be due to numerous tourists walking in the area during daylight, we counted over 300 people in individual images, moving while drone acquisitions are made. We attempted to reduce this effect by flying the drone in the very early morning hours (5 a.m. local time), which however may also be the timing of larger steam degassing. An increased steaming of thermal fields in the morning hours has been described elsewhere, and is thought to be associated with reduced air pressure (Bredemeyer and Hansteen, 2014). Therefore, digital elevation models and photomosaic from optical data might show some bias near to the most pronounced thermal sites, such as Strokkur and Great Geysir.

The infrared imagery was excessive (several thousands of images) and therefore challenging to handle. Moreover, the thermal images, recorded in 16-bit radiometric format provided us with the possibility to correct for atmospheric and geometric effects. The distance to the ground was assessed and corrected, the emissivity was defined. We then selected a fixed color scale and saved all images in non-radiometric format. These images were then processed in the Structure from Motion (SfM) scheme, and a thermal field mosaic as well as a DEM generated. The data, available on request, after this procedure are non-radiometric, however. This way of enhancing contrasts was found to be necessary for retrieving enough feature points in the SfM data processing. As a result, further details on

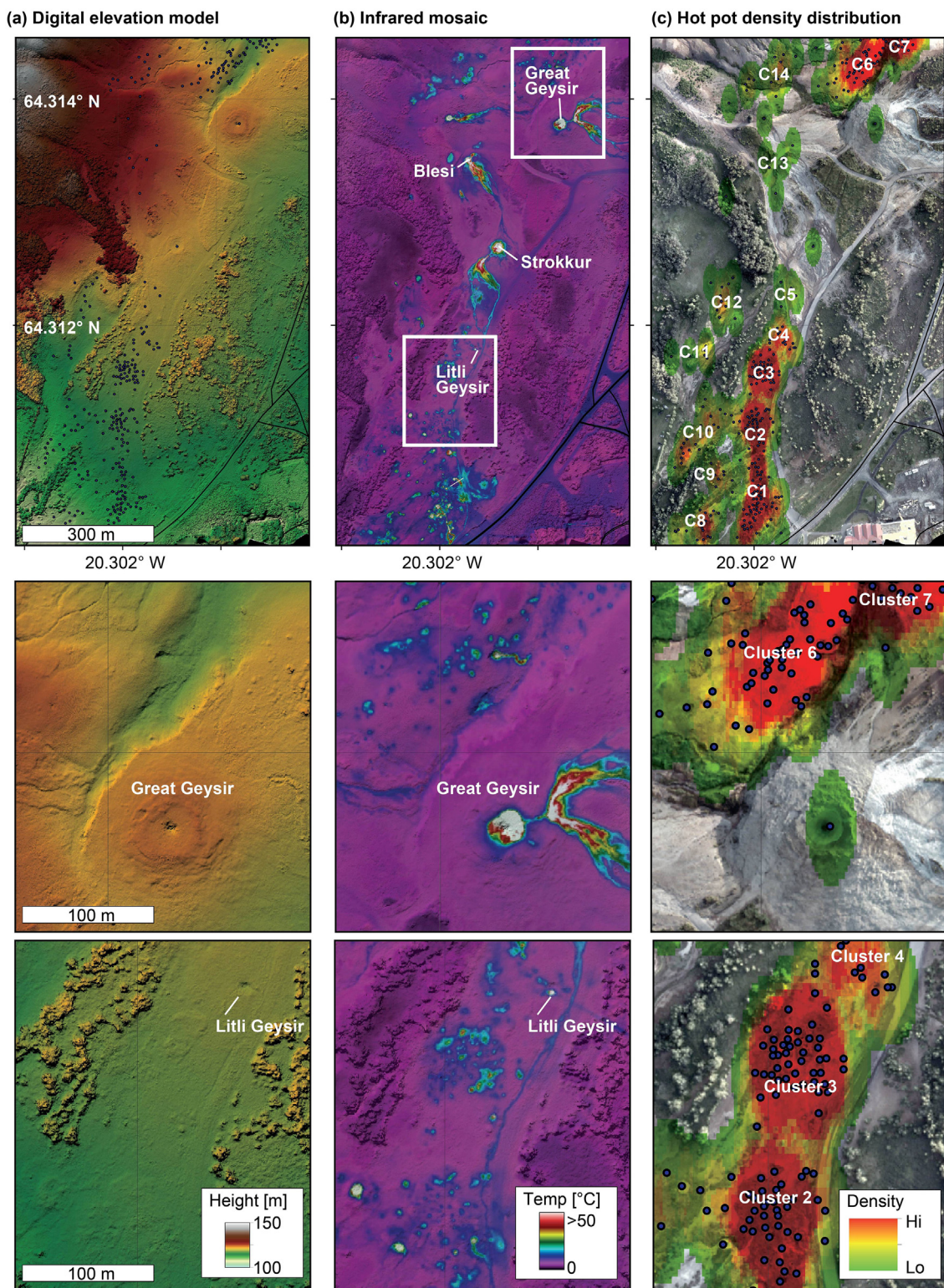


Fig. 4. Close-up views of drone-based results. Left column shows digital elevation model, centre column is the infrared aero-mosaic, and right column shows the distribution of hot pots (black dots) and the results from the cluster analysis (green-red colored). Top row is overview, the bottom rows show zoom-ins as indicated by white boxes in infrared mosaic overview (b, top row). Note that hot pot density distribution shows that they often appear clustered, unless an open geyser has punctuated the surface. Maps generated by authors using ArcMap 10.2 by ESRI (<http://www.esri.com/>).

the energy budget of the different hot spot clusters and the geysers cannot be retrieved from the result presented herein and will be more detailed in a separate study.

Orientations of drone photos, both radiometric and optical, are roughly geolocated using internal GPS, and further improved using

differential GPS measured ground control points. The underwater camera views, however, do not permit a similar approach. The orientation of the underwater camera was changing while plunging the camera, especially near to the elongated crack-like expression at 9–12 m depth. At this depth, the water column is highly unstable and turbulent and

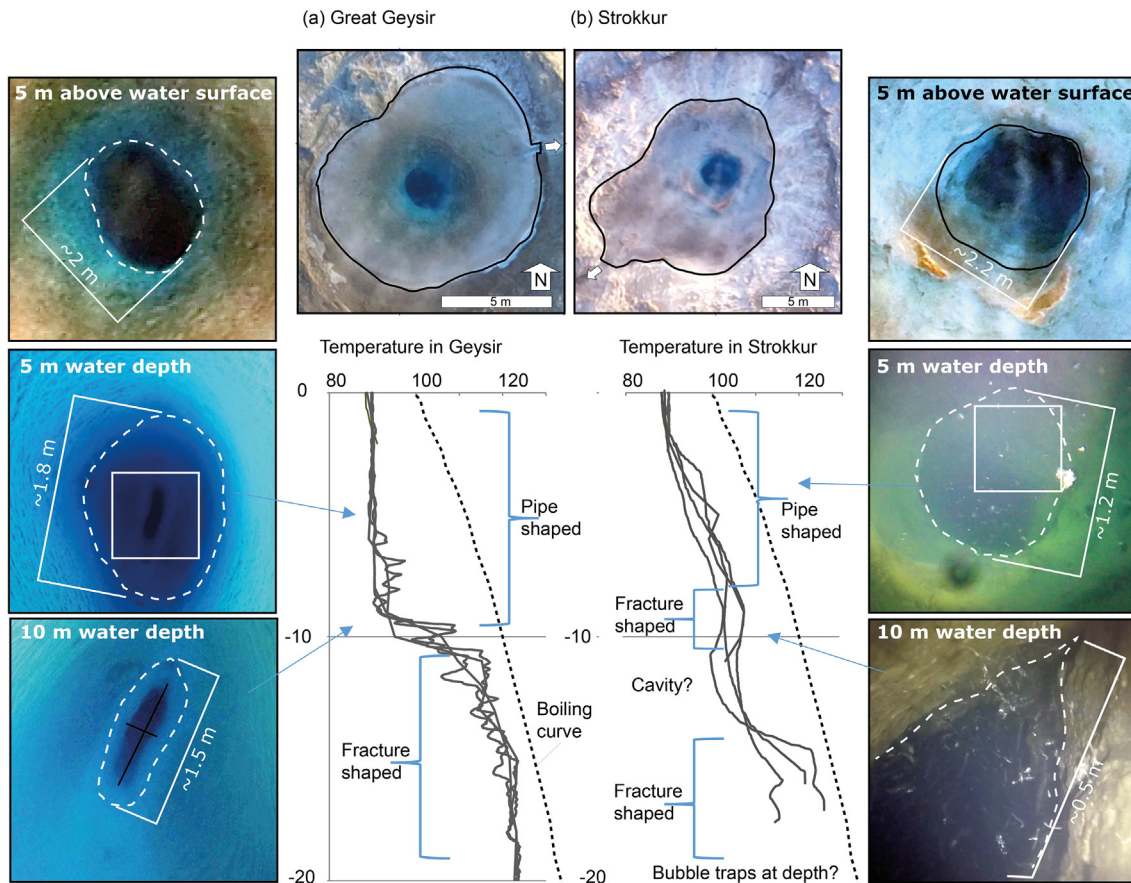


Fig. 5. Results from drone optical camera and underwater camera observations at Great Geysir (left) and Strokkur (right), and comparison to water temperature logs. At the surface, a preferred direction of the geyser pipes is hardly identifiable, as the drone photos from 10 m and 5 m height show. Outflow channels at Great Geysir to the E, at Strokkur to the SW, indicated by white arrow in drone images (top row). Drone photo from Strokkur at 5 m height level shows quadratic structure, which is a concrete cellar remnant of the drilling project in 1963. Underwater photographs (left Great Geysir, right Strokkur), show for both geysers first a sintered near circular pipe, becoming elongated at 9–12 m depth. The vertex region of the major axis is crack-like, as the images at 12 m show, implying a structural control. Temperature comparison reveals that narrowing or fracture like geometry of the pipe is associated with increases in water temperature. At depth of 13–15 m, both geyser temperatures are closest to theoretical boiling temperature (dashed line). Water depth was determined by pressure sensor. All photos taken during the field work by the authors. Profiles created by authors using MATLAB R2013 (www.mathworks.com).

convective streams rotate the camera. Therefore the accurate direction of the elongated fissure might contain an uncertainty. Therefore we traced the direction by acquiring a video from above the water to larger depth, and sequentially identify the location and azimuths of feature points. Nevertheless, future studies might improve this data handling by adding dedicated markers at depth.

The depth of the underwater camera was obtained by measuring the length of the dyneema line below the water table. Whether the line was bending or otherwise deflecting from the vertical could not be assessed. However, due to the weight of the underwater camera (2.4 kg in total) we assume that the line was straight and our depth measurements appropriate. Future attempts might use a pressure sensor simultaneously, so that precise depths information could be retrieved. However, the temperatures of 120 °C or more at this depth will remain challenging for any electronic and battery driven device. Nevertheless, the cameras showed tremendous differences to the simple radial-symmetric geyser pipe measured with a 3-arm caliper tool earlier (Torfason, 1985), as here we could reveal crack-like, highly elongated fractures. The temperature profiles shown were taken between geyser eruptions, and can therefore be considered as minimum temperatures.

4.2. Implications

Previous studies of geysers have suggested that their location is controlled by lithology and geology (Belousov et al., 2013). The present study implies that the presence and orientation of faults matters. A

large number of historic documents describe the increased activity at geysers following earthquakes (Torfason, 1985; Wang and Manga, 2010). Also on Iceland, the geysers and hot springs have repeatedly shown a triggered response following tectonic earthquake activity (Hurwitz and Lowenstern, 2014; Husen et al., 2004; Rinehart, 1980; Thorkelsson, 1925), and now our study reveals the presence of fractures or faults at depth, that may have provided the permeable pathways for water fluids and gas bubbles (see Fig. 6). Unfortunately, no such earthquake-geyser interactions at the Geysir geothermal field has been instrumentally recorded yet, which is why we did not further elaborate on this. Earthquake in the vicinity of the geyser field typically originate in southern Iceland, on average once per century, such as the 2000 strike slip earthquake that occurred in the South Iceland Seismic Zone (SISZ). Already in the year 1294, earthquakes have led to significant activity changes in the area, shutting down some and leading to the eruption of other geysers and hot springs (Pasvanoglu, 1998). Also much later, in 1640, the Great Geysir was awakened and erupted violently after a 40 year dormancy. The activity at the Great Geysir was then low again, few eruptions per year only, until in 1896 a tectonic earthquake reawakened it again, erupting several times per day then, some even reaching 60 m height (Pasvanoglu, 1998). In the year 2000, two earthquakes Mw6.5 and Mw6.3 occurred in close succession, which have themselves been identified as interacting events (Arnadottir et al., 2003; Bonafede et al., 2007). Shortly after, the Hengill region displayed triggered microseismicity (Antonioli et al., 2006; Vogfjord, 2003), as did the region surrounding the Geysir field (see also Fig. 1). In addition, it

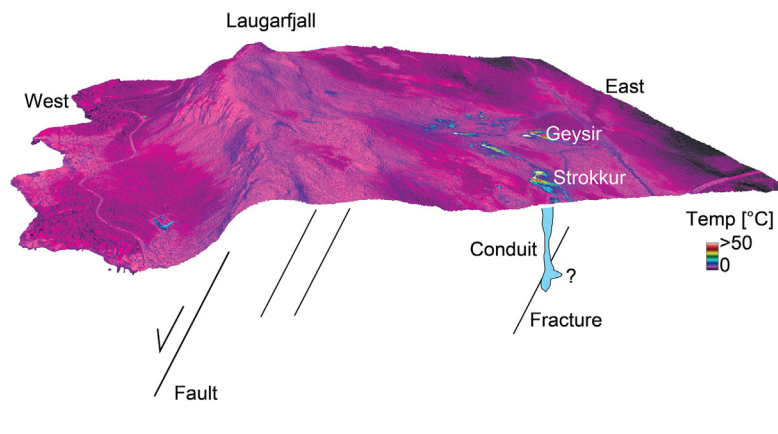


Fig. 6. Sketch with schematic perspective view (not to scale) over Laugarfjall and the Geysir geothermal field. Laugarfjall is structurally delimited by a normal fault on its western side, azimuth NNE-SSW. Local fracture lineaments near the Geysir geothermal field, as well as alignments of hot pot clusters and underwater photography reveals a structural control as well. We note that similar azimuths have been identified from triggered microseismicity in 2000, implying a possible triggering effect at buried fractures and herewith also at the geysers. For map dimensions we refer to Fig. 3, scale of conduit see in Fig. 5. Map generated by authors using ArcMap 10.2 by ESRI (<http://www.esri.com/>).

was reported that Great Geysir had a large eruption after a long period of dormancy, as well as Strokkur and a number of the smaller hot springs (Litli Strokkur, Litli Geysir and others) (Palmason, 2002). However, these are eyewitness records that have not been documented by geophysical or geochemical monitoring data. Only by continuous monitoring, we would be able to decipher if such relationships are true or coincident, especially because the present eruption frequency of the Great Geysir is poorly known (during our fieldworks we witnessed eruptions, see Fig. 1c). Considering that the 2000 earthquakes triggered microseismicity at NNE-SSW trending faults in the Geysir geothermal field (Hjaltadóttir, 2009), and considering that the geysers and hot springs are structurally controlled as well, we may conjecture different possibilities explaining the triggered activity at the Geysir field. (i) The dynamic waves passing through the geysers and hot springs leads to a conjoint activity increase, and/or (ii) the fault and fractures systems are triggered which themselves provide permeability zones that feed the Geysir field. The latter, specifically, is not a direct triggering effect but rather displays a cascade of events, initiating with the earthquakes, fault triggering by seismic waves, which themselves may host and be the pathway for hydrothermal fluids that are directly linked to the geysers and hot springs. Only such a cascade would also explain why a large number of the Geysir field expulsions showed an activity change. As triggered geyser activity changes are observed worldwide (Ingebritsen and Rojstaczer, 1996), a closer search for the cascading processes is desirable for understanding the processes at these geothermal sites. Even small triggers, such as induced by acoustic noise, may activate a geyser (Alexandrov et al., 2016). Especially as geysers are considered as a multiphase volcano analogue (water-steam-solid), understanding the geyser-tectonic interactions, identification of clustered and aligned piercing points and relationships to earthquakes might also be applied to or stimulate further volcano research (Karlstrom et al., 2013). At both, geysers and volcanoes, conduit geometry and conduit processes are monitored and help understanding subsurface dynamics (Vandemeulebrouck et al., 2014). At the Geysir field of Iceland, we could for the first time obtain detailed views into the conduit, revealing a fracture-controlled geometry at depth and circular geometry in the upper ~8–10 m. Similarly also a recent study from Chile could identify a fissure-like geometry at depth, and a conduit-like geometry at the surface (Muñoz-Saez et al., 2015a). Fault control and complexities in conduit geometries affect the friction resistance to the water/steam flow, and therefore also the eruption dynamics of geysers. The deterministic and stochastic dynamics is controlled by the friction coefficient (which depends on conduit geometry and morphology) and the relative pressure (Alexandrov et al., 2016), which are becoming quantifiable by video observations as this study demonstrated.

At the final stages of our video recordings, we can only weakly identify the conduit walls (see Supplementary information). A careful inspection of our video shows a possible widening of the conduit geometry at depth and presence of reservoirs and more inclined and horizontal conduits. Future video recordings will allow more detailed investigation of the complexities in the geometry at depth, which may provide bubble traps as proposed elsewhere (Belousov et al., 2013; Muñoz-Saez et al., 2015b; Vandemeulebrouck et al., 2014).

The photogrammetric data presented is a snap shot of the situation as it was in 2016. During our field work we found that eruptions at Strokkur have a periodicity of 3–7 min for single eruptions, and 12–35 min for double eruptions (two eruptions that occur in close temporal proximity), possibly indicating complexities in the geometry of the bubble traps at depth. Moreover, time dependent variations may also occur in space, such as the expression and location of hot pots and the geysers could change and would require repeat measurements. Potentially, repeat measurements could be realized not only from the drone, but also inside the conduit, in order to monitor changes occurring with time. Therefore the present results are an important benchmark for future studies as well.

5. Conclusions

For the first time a detailed drone based photogrammetric and infrared mapping project was realized at the Geysir geothermal field, and thousands of close range photographs analyzed by using the Structure from Motion algorithm. We generated a centimeter scale digital elevation and thermal anomaly map, and could count 364 distinct thermal anomalies, that show a clustered appearance, and isolated piercing points of the larger geysers, i.e. Strokkur and Great Geysir. The thermal clusters follow a trend that is NNE-SSW, parallel to triggered microseismicity after the 2000 earthquakes in southern Iceland, and parallel to the NNE-SSW regional tectonic trend that is identified on elevation data. Underwater camera records reveal also that the conduits of the two largest geysers, Strokkur and Great Geysir itself, are at depth of 9–12 m becoming constricted, fracture-controlled, and their cross sections elongated. At this depth the boiling temperature is reached for the first time, meaning that steam bubbles must form at this depth or deeper. At depths exceeding 16 m the geyser pipe geometry complicates, diverges into several branches and cavities. This study therefore highlights the important geological structural control on geyser and hot spring distribution, as well as their feeding system, and may also help understanding how remote tectonic earthquakes may activate these structures through fault process activation, and change a large number of the thermal expressions at the surface.

Acknowledgements

We thank the Environment Agency of Iceland for research permit at the Geysir geothermal field, specifically Lárus Kristjánsson and Sigrún Ágústsdóttir and especially also the park rangers for their support and interest in our work. This work contributed and was partially supported by the FUTUREVOLC project and IMAGE project. This is a contribution to VOLCAPSE, a research project funded by the European Research Council under the European Union's H2020 Programme / ERC consolidator grant n. [ERC-CoG 646858]. Moreover we thank the DLR for providing the TanDEM-X data set was used to derive a topographic base map of the region. Finally, we thank the reviewers (Alexander Belousov, Michael Manga and anonymous) for constructive comments and help improving the paper, and Kristján Sæmundsson and Benedikt Steingrímsson, both at ISOR for reading the manuscript and making useful.

Appendix A. Supplementary data

Supplementary data associated with this article can be found in the online version, at <https://doi.org/10.1016/j.jvolgeores.2018.01.010>. These data include the Google map of the most important areas described in this article.

References

- Alexandrov, D., Bashkirtseva, I., Ryashko, L., 2016. Analysis of noise-induced eruptions in a geyser model. *Eur. Phys. J. B* 89 (62), 8.
- Amici, S., Turci, M., Giulietti, F., Giannanco, S., Buongiorno, M.F., La Spina, A., Spampinato, L., 2013. Volcanic environments monitoring by drones mud volcano case study. *Int. Arch. Photogramm. 5–10.*
- Antonioli, A., Belardinelli, M.E., Bizzarri, A., Vogfjord, K.S., 2006. Evidence of instantaneous dynamic triggering during the seismic sequence of year 2000 in south Iceland. *J. Geophys. Res. Solid Earth* 111 (B3).
- Arnadottir, T., Jonsson, S., Pedersen, R., Gudmundsson, G.B., 2003. Coulomb stress changes in the South Iceland Seismic Zone due to two large earthquakes in June 2000. *Geophys. Res. Lett.* 30 (5).
- Balcerak, E., 2013. Linking earthquakes and hydraulic fracturing operations. *Eos Trans. AGU* 94 (1), 3.
- Bart, T.F.W., 1940. *Geysir in Iceland*. Am. J. Sci. 238 (6), 381–407.
- Belousov, A., Belousova, M., Nechayev, A., 2013. Video observations inside conduits of erupting geysers in Kamchatka, Russia, and their geological framework: implications for the geyser mechanism. *Geology* 41 (4), 387–390.
- Bonafede, M., Ferrari, C., Maccaferri, F., Stefansson, R., 2007. On the preparatory processes of the M6.6 earthquake of June 17th, 2000, in Iceland. *Geophys. Res. Lett.* 34 (24).
- Bredemeyer, S., Hansteen, T.H., 2014. Synchronous degassing patterns of the neighbouring volcanoes Llaima and Villarrica in south-central Chile: the influence of tidal forces. *Int. J. Earth Sci.* 103 (7), 1999–2012.
- Bunsen, R., 1847. Über den inneren Zusammenhang der pseudovulkanischen Erscheinungen Islands. Wöhlers und Liebigs Annalen der Chemie und Pharmacie LXII, pp. 1–59.
- Carrivick, J.L., Smith, M.W., Quincey, D.J., Carver, S.J., 2013. Developments in budget remote sensing for the geosciences. *Geol. Today* 29 (4), 138–143.
- Dowden, J., Kapadia, P., Brown, G., Rymer, H., 1991. Dynamics of a geyser eruption. *J. Geophys. Res. Solid Earth* 96 (B11), 18059–18071.
- Duncel, A.E., Cardenas, M.B., Sawyer, A.H., Bennett, P.C., 2009. High-resolution in-situ thermal imaging of microbial mats at El Tatio Geyser, Chile shows coupling between community color and temperature. *Geophys. Res. Lett.* 36.
- Einarsson, T., 1967. The Great Geysir and the Hot Spring-area of Haukadalur, Iceland. 24. The Geysir Committee.
- Hjaltadóttir, S., 2009. Use of Relatively Located Microearthquakes to Map Fault Patterns and Estimate the Thickness of the Brittle Crust in Southwest Iceland. University of Iceland, Reykjavik (104 pp.).
- Hjartardottir, A.R., Einarsson, P., Bjorgvinsdottir, S.G., 2016. Fissure swarms and fracture systems within the Western Volcanic Zone, Iceland – effects of spreading rates. *J. Struct. Geol.* 91, 39–53.
- Hurwitz, S., Lowenstern, J.B., 2014. Dynamics of the Yellowstone hydrothermal system. *Rev. Geophys.* 52 (3), 375–411.
- Hurwitz, S., Manga, M., 2017. The fascinating and complex dynamics of geyser eruptions. *Annu. Rev. Earth Planet. Sci.* 45 (45), 31–59.
- Husen, S., Taylor, R., Smith, R.B., Heasler, H., 2004. Changes in geyser eruption behavior and remotely triggered seismicity in Yellowstone National Park produced by the 2002 M 7.9 Denali fault earthquake, Alaska. *Geology* 32 (6), 537–540.
- Hutchinson, R.A., Westphal, J.A., Kieffer, S.W., 1997. In situ observations of Old Faithful Geyser. *Geology* 25 (10), 875–878.
- Ingebritsen, S.E., Rojstaczer, S.A., 1993. Controls on geyser periodicity. *Science* 262 (5135), 889–892.
- Ingebritsen, S.E., Rojstaczer, S.A., 1996. Geyser periodicity and the response of geysers to deformation. *J. Geophys. Res. Solid Earth* 101 (B10), 21891–21905.
- James, M.R., Varley, N., 2012. Identification of structural controls in an active lava dome with high resolution DEMs: Volcán de Colima, Mexico. *Geophys. Res. Lett.* 39 (22), L22303.
- Jones, B., Renaut, R.W., Torfason, H., Owen, R.B., 2007. The geological history of Geysir, Iceland: a tephrochronological approach to the dating of sinter. *J. Geol. Soc. Lond.* 164, 1241–1252.
- Julian, B.R., 1998. Eruption dynamics – rumbling geysers (and volcanoes). *Nature* 396 (6709), 311.
- Karlstrom, L., Hurwitz, S., Sohn, R., Vandemeulebrouck, J., Murphy, F., Rudolph, M.L., Johnston, M.J.S., Manga, M., McCleskey, R.B., 2013. Eruptions at Lone Star Geyser, Yellowstone National Park, USA: 1. Energetics and eruption dynamics. *J. Geophys. Res. Solid Earth* 118 (8), 4048–4062.
- Kieffer, S.W., 1984. Seismicity at Old Faithful Geyser: an isolated source of geothermal noise and possible analogue of volcanic seismicity. *J. Volcanol. Geotherm. Res.* 22, 59–95.
- Mackenzie, G.S., 1842. *Travels in Iceland*. Chambers, Edinburgh, Scotland.
- Malin, R.A., Franks, M., Pierce, S.A., 2011. Using Forward Looking Infrared (FLIR) imagery to gauge thermal flux: preliminary method development and evaluation applied to the El Tatio geyser field. *Sensors* 16 (1518), 980–982.
- Mancini, F., Dubbini, M., Gattelli, M., Stecchi, F., Fabbri, S., Gabbianielli, G., 2013. Using unmanned aerial vehicles (UAV) for high-resolution reconstruction of topography: the structure from motion approach on coastal environments. *Remote Sens.* 5 (12), 6880–6898.
- Manga, M., Brodsky, E., 2006. Seismic triggering of eruptions in the far field: volcanoes and geysers. *Annu. Rev. Earth Pl. Sc.* 34, 263–291.
- Munoz-Saez, C., Manga, M., Hurwitz, S., Rudolph, M.L., Namiki, A., Wang, C.Y., 2015a. Dynamics within geyser conduits, and sensitivity to environmental perturbations: insights from a periodic geyser in the El Tatio geyser field, Atacama Desert, Chile. *J. Volcanol. Geotherm. Res.* 292, 41–55.
- Munoz-Saez, C., Namiki, A., Manga, M., 2015b. Geyser eruption intervals and interactions: examples from El Tatio, Atacama, Chile. *J. Geophys. Res. Solid Earth* 120 (11), 7490–7507.
- Nakano, T., Kamiya, I., Tobita, M., Iwashashi, J., Nakajima, H., 2014. Landform monitoring in active volcano by Uav and Sfm-Mvs technique. *Isprs Technical Commission Viii Symposium.* 40–8, pp. 71–75.
- Neale, C.M.U., Jaworowski, C., Heasler, H., Sivarajan, S., Masih, A., 2016. Hydrothermal monitoring in Yellowstone National Park using airborne thermal infrared remote sensing. *Remote Sens. Environ.* 184, 628–644.
- Pálmarson, G., 2002. Iceland's Geysir aroused by earthquakes in June 2000. *The GOSA Transactions.* 7, pp. 139–147.
- Pantaleo, M., Walter, T.R., 2014. The ring-shaped thermal field of Stefanos Crater, Nisyros Island: a conceptual model. *Solid Earth (SE, Gottingen)* 5 (1), 183–198.
- Pasvanoglu, S., 1998. Geochemical study of the Geysir geothermal field in Haukadalur, Iceland. In: U.N. University (Ed.), *Geothermal Training Programme. Proceedings World Geothermal Congress 2000 Reykjavik, Iceland*, pp. 281–318.
- Rinehart, J.S., 1980. *Geysers and Geothermal Energy*. Springer-Verlag (223 pp.).
- Rojstaczer, S.A., Ingebritsen, S.E., Hayba, D.O., 2008. Permeability of continental crust influenced by internal and external forcing. *Geofluids* 8 (2), 128–139.
- Sigmundsson, F., 2006. *Iceland Geodynamics: Crustal Deformation and Divergent Plate Tectonics*. Springer, Berlin, pp. 1–214.
- Spampinato, L., Calvari, S., Oppenheimer, C., Boschi, E., 2011. Volcano surveillance using infrared cameras. *Earth-Sci. Rev.* 106 (1–2), 63–91.
- Storm, G., 1888. Oddverjaanna'll. In: Groendahl, C. (Ed.), *Islandske Annaler indtil 1578, Oslo*, pp. 427–491.
- Thorkelson, T., 1925. On thermal activity in Iceland and geyser action. *Soc. Sci. Isl. XXV*, 139.
- Torfason, H., 1985. The Great Geysir. *Geysir Conservation Committee, Reykjavik*, p. 23.
- Torfason, H., 1999. Geology of the Geysir area in southern Iceland. *Proceedings of the 5th International Symposium on the Geochemistry of the Earth's Surface (GES-5)*, pp. 2–5.
- Vandemeulebrouck, J., Sohn, R.A., Rudolph, M.L., Hurwitz, S., Manga, M., Johnston, M.J.S., Soule, S.A., McPhee, D., Glen, J.M.G., Karlstrom, L., Murphy, F., 2014. Eruptions at Lone Star geyser, Yellowstone National Park, USA: 2. Constraints on subsurface dynamics. *J. Geophys. Res. Solid Earth* 119 (12), 8688–8707.
- Vogfjord, K.S., 2003. Triggered seismicity in SW Iceland after the June 17, Mw = 6.5 earthquake in the South Iceland Seismic Zone: the first five minutes, EGU. *Geophysical Research Abstracts*, Nice, p. 11251.
- Wang, C.Y., Manga, M., 2010. Hydrologic responses to earthquakes and a general metric. *Geofluids* 10 (1–2), 206–216.
- Wu, S.-M., Ward, K.M., Farrell, J., Lin, F.-C., Karplus, M., Smith, R.B., 2017. Anatomy of Old Faithful from subsurface seismic imaging of the Yellowstone Upper Geyser Basin. *Geophys. Res. Lett.* 44, 10,240–210,247.